Atmospheric
Chemistry
and Physics
Discussions

Local and remote temperature response of regional SO$_2$ emissions

Anna Lewinschal[1,2], Annica M. L. Ekman[1,2], Hans-Christen Hansson[2,3], Maria Sand[4], Terje
K. Berntsen[4,5], and Joakim Langner[6]

[1]Department of Meteorology, Stockholm University, Stockholm, Sweden
[2]The Bolin Centre for climate research, Stockholm University, Stockholm, Sweden
[3]Department of Environmental Science and Analytical Chemistry, Stockholm University, Stockholm, Sweden
[4]CICERO Center for International Climate and Environmental Research, Oslo, Norway
[5]University of Oslo, Department of Geosciences, Oslo, Norway
[6]Swedish Meteorological and Hydrological Institute, Air Quality Research Unit, Norrköping, Sweden

Correspondence: Anna Lewinschal (anna@misu.su.se)

1 **Abstract.** Short-lived anthropogenic climate forcers, such as sulphate aerosols, affect both climate and air quality. Despite

2 being short-lived, these forcers do not affect temperatures only locally; regions far away from the emission sources are also

3 affected. Climate metrics are often used e.g. in a policy context to compare the climate impact of different anthropogenic

4 forcing agents. These metrics typically relate a forcing change in a certain region with a temperature change in another region

5 and thus often require a separate model to convert emission changes to radiative forcing changes.

6   In this study, we used a coupled Earth System Model (NorESM) to calculate emission-to-temperature-response metrics for

7 sulphur dioxide (SO$_2$) emission changes in four different policy-relevant regions: Europe, North America, East Asia and South

8 Asia. We first increased the SO$_2$ emissions in each individual region by an amount giving approximately the same global

9 average radiative forcing change (-0.45 Wm^{-2}). The global mean temperature change per unit sulphur emission compared to

10 the control experiment was independent of emission region and equal to ~0.006K/TgSyr^{-1}. On a regional scale, the Arctic

11 showed the largest temperature response in all experiments. The second largest temperature change occurred in the region of

12 the imposed emission increase, except when South Asian emissions were changed; in this experiment, the temperature response

13 was approximately the same in South Asia and East Asia. We also examined the non-linearity of the temperature response by

14 removing all anthropogenic SO2 emissions over Europe in one experiment. In this case, the temperature response (both global

15 and regional) was twice of that in the corresponding experiment with a European emission increase. This nonlinearity in the

16 temperature response is one of many uncertainties associated with the use of simplified climate metrics.

17 *Copyright statement.* TEXT

1 Introduction

19 Anthropogenic emissions of short-lived climate forcers (SLCFs), i.e. chemical components in the atmosphere that interact

20 with radiation, have both an immediate effect on local air quality and regional and global effects on the climate in terms of

Atmospheric
Chemistry
and Physics
Discussions

21 e.g. changes in the temperature and precipitation distribution. Aerosol particles are one of the most important SLCFs due to

22 their abundance and their effects on health and climate. The short atmospheric residence times of SLCFs such as sulphate

23 and carbonaceous aerosols (around days) lead to high atmospheric concentrations in emission regions and a highly variable

24 radiative forcing pattern. Regional radiative forcing can, nevertheless, exert a large influence on the temperature field away

25 from the forcing region through changes in heat transport or the atmospheric or ocean circulation (Menon et al., 2002; Shindell

26 et al., 2010; Lewinschal et al., 2013; Acosta Navarro et al., 2016; Dong et al., 2016). Here, we investigate the effect of sulphate

27 aerosol precursor emission perturbations in different regions on the global surface temperature distribution using a global

28 climate model.

29   The local radiative forcing by a unit aerosol emission varies from region to region depending on a number of factors,

30 including e.g. emission location, aerosol processing in the atmosphere and removal rates as well as land surface properties and

31 cloud distribution (e.g. Bellouin et al., 2016). Moreover, a unit radiative forcing in a specific region may have different impacts

32 on the temperature response locally in the forcing region and in remote regions away from the forcing, as well as between

33 different remote regions. In other words, the climate sensitivity in one region can vary depending on the location of the forcing

34 (e.g. Shindell and Faluvegi, 2009).

35   To facilitate comparisons of the climate effect of different greenhouse gases and emission levels, several climate metrics

36 have been developed which connect emission changes to radiative forcing, or a specified forcing to a temperature response

37 (e.g. Aamaas et al., 2013). One appeal of simple climate metrics is that they provide a way to easily evaluate the climate impact

38 of different air quality or climate mitigation policies without having to run a coupled climate model, something which is not

39 always feasible due to the computational costs. Because of the even spatial distribution of long lived greenhouse gases, these

40 metrics have usually described global average quantities. However, the highly variable spatial distribution of aerosol forcing

41 necessitates the use of metrics that take these spatial inhomogeneities into account (Shine et al., 2005).

42   Shindell and Faluvegi (2009) developed a metric that accounts for spatial inhomogeneities both in the forcing and tempera-

43 ture response, the Regional Temperature Potential (RTP). With a large set of simulations with one climate model, where they

44 varied the location of forcing from various anthropogenic climate forcers, these authors derived RTP coefficients that link the

45 radiative forcing from a climate forcer in a specific region to regional temperature responses. An evaluation of the method for

46 transient simulations of historical aerosol forcing and response with four different climate models was presented in the work

47 of Shindell (2012).

48   However, the simplification inherent in the climate metric concept might lead to difficulties related to the generality of these

49 metrics, such as the RTP. Differences between RTP coefficients derived from different climate models can stem from a number

50 of different sources, involving everything from atmospheric processing of aerosols, interaction with radiation, aerosol cloud

51 effects or climate feedbacks, and how these processes are represented in different climate models (Kasoar et al., 2016).

52   The main objective of this study is to investigate the global and remote impacts of regional sulphate aerosol precursor

53 emission changes on the surface temperature distribution. This is done by using a coupled atmosphere-ocean model with

54 interactive aerosol representation, the Norwegian Earth System Model (NorESM). The results from the model simulations are

55 used to derive RTP coefficients similar to the work of Shindell and Faluvegi (2009). However, our method for deriving RTP

Atmospheric
Chemistry
and Physics
Discussions

56 coefficients differs from that of Shindell and Faluvegi (2009) in that we derive our RTP coefficients directly from emission
57 perturbations and focus primarily on the emissions-temperature connection rather than the connection between radiative forcing
58 and temperature. The RTP coefficients derived by Shindell and Faluvegi (2009) describe the regional temperature change in
59 response to regional radiative forcing, and essentially describe a regional sensitivity. These forcing-based sensitivities have to
60 be combined with the radiative forcing patterns derived from emission scenarios with a chemistry transport model or offline
61 calculations for radiative forcing with a general circulation model to provide the emission-temperature connection. Another
62 difference is that we focus on emissions from air-pollution and policy-making relevant regions rather than the latitudinal bands
63 of Shindell and Faluvegi (2009). Thus, we seek to investigate how much an emission change in one policy relevant region
64 affects both local climate as well as the climate on global scale and in remote regions.

65   The aim is that the RTP coefficients derived with NorESM eventually could be used in Integrated Assessment analysis
66 (IAA), e.g. such as the Greenhouse gas - Air pollution Interactions and Synergies (GAINS) model. In the GAINS model the
67 climate impact is estimated using the Global Warming Potential (GWP), which is the global radiative forcing integrated over
68 time normalised by that of CO_2 (Amann et al., 2011). By the GWP the global climate impact of SLCFs can be taken into
69 account. Lately the radiative forcing of long-lived greenhouse gas emission changes due to air pollution abatement, other than
70 CO_2, has been included. Using RTP coefficients in IAA would mean that not only near-term climate effects of changed SLCF
71 emissions can be evaluated but also how different regions are affected due to specific regional abatement measures. The RTP
72 can be based on different entities as radiative forcing, effective radiative forcing or direct emissions, which need very different
73 support calculations respectively. Using the emissions as base for RTPs will provide a very simple way to estimate the climate
74 impact of changed emissions without having to run a chemical transport model. Using any of the bases for the RTPs avoids
75 running large coupled climate models. However, the validity of this method relies on the accuracy of the assumption that the
76 temperature response to changed emissions is linear and that the interaction between different SLCF are negligible for the
77 resulting temperature response. To address the question regarding linearity in the response depending on emission perturbation
78 strength we perform simulations with different emission perturbations for the European region.

79   The layout of this study is as follows. First an introduction to the RTP methodology is presented in the method section. The
80 NorESM model is described together with the experimental design to derive the emission specific RTP coefficients. In Sect.
81 3 we first present the results from experiments where sulphate aerosol precursor emissions were increased and the global and
82 regional effect of these emission perturbations. The results of an experiment where European anthropogenic sulphate aerosol
83 precursor emissions were removed are discussed in the context of non-linearities emerging as a consequence of emission mag-
84 nitudes. Last in the Result section is an comparison of the performance of the forcing-based RTP coefficients of Shindell and
85 Faluvegi (2009) and Shindell et al. (2012) for NorESM results. The Result section is followed by a discussion and conclusions.

2 Method

2.1 The Absolute Regional Temperature Potential

88 There exists a number of different climate metrics that describe the connection between emissions of atmospheric tracer species

89 and/or their radiative forcing and/or their effect on the global mean temperature. Many have been developed for the purpose

90 of evaluating the impact of increased emissions of long-lived and well-mixed greenhouse gases. Thus, the connection between

91 the location of an emission perturbation and the temperature response has not been a primary concern. However, for SLCFs

92 the location of the emission perturbation and radiative forcing is a primary matter of interest. A climate metric which takes the

93 spatial distribution of these SLCFs and the temperature response into account was developed by Shindell and Faluvegi (2009)

94 and Shindell and Faluvegi (2010). The metric describes the temperature change dT in one area a at time t, in response to

95 forcing F in area a':

$$dT_a(t) = \int_0^t \left(\sum_{a'} F_{a'}(t') \cdot \frac{dT_a/F_{a'}}{dT_a/F_{global}} \right) \cdot IRF(t-t')dt', \qquad (1)$$

96 where the numerator in the second term of the sum, $dT_a/F_{a'}$, is the regional response coefficient (cf. Table 3 of Shindell

97 and Faluvegi (2010)), which, in this formulation is normalised by the regional temperature response to global average forcing,

98 dT_a/F_{global}. The Impulse Response Function, IRF, represents the time dependent temperature response per unit forcing, i.e.

99 the climate sensitivity. For the equilibrium (or quasi-equilibrium or transient) temperature response to a steady forcing, the

100 IRF can be replaced by the equilibrium or transient climate sensitivity, λ.

101 Shindell (2012) elaborated the regional temperature change metric of Shindell and Faluvegi (2010) to an Absolute Regional

102 Temperature potential, $ARTP$, which, in analogue to the Absolute Global Temperature change Potential (AGTP), connects an

103 emission perturbation, E, in region r of a climate forcer to an absolute temperature change (Shine et al., 2005) in area a:

$$ARTP_{a,r}(t) = \int_0^t \left(\sum_{a'} \frac{F_{a'}(t')}{E_r} \cdot \frac{dT_a/F_{a'}}{dT_{global}(F_{global})/F_{global}} \right) \cdot IRF(t-t')dt'. \qquad (2)$$

104 This formulation uses the global climate sensitivity $(dT_{global}(F_{global})/F_{global})$ to normalise the regional response coeffi-

105 cients in contrast to Eq. 1 which uses the regional sensitivity to global forcing. This, i.e. the second term in the summation of

106 Eq. 2, yields the unitless RTP coefficients presented in Table 1 of Shindell (2012). Shindell (2012) also advocate the use of the

107 latter formulation (Eq. 2) before the former (Eq. 1).

108 The RTP coefficients provided in the work of Shindell and Faluvegi (2010) and Shindell (2012) were derived for forcing in

109 four latitude bands covering the globe: the Southern Hemisphere extratropics (90-28°S, SHext), Tropics (28°S-28°N), Northern

110 Hemisphere mid latitudes (28-60°N, NHml) and Arctic (60-90°N). These RTP coefficients can be used to estimate the global

111 temperature response to any emission perturbation, as long as the forcing in response to the emission perturbation in each of

Atmospheric
Chemistry
and Physics
Discussions

Open Access

EGU

112 the latitude bands described above is known. The forcing distribution in response to an emission perturbation can be calculated

113 with e.g. a chemistry transport model (direct radiative forcing only), or with atmospheric general circulation models.

114   In this work, we take our starting point in emission perturbations rather than in the forcing distribution. Sub-global tem-

115 perature changes in response to emission perturbations are derived both for latitudinal bands following Shindell and Faluvegi

116 (2009) as well as for the emission regions defined in this study, with the addition of a complementary Arctic region (AR).

117 This complementary Arctic region is defined as the area north of the Arctic circle (66°N), whereas the northernmost latitudinal

118 band (hereafter denoted ARCT) is defined as the area north of 60°N in accordance with the definition of Shindell and Faluvegi

119 (2009). All regions that are used in this study are listed in Table 1.

120 2.2 NorESM

121 The regional temperature changes in response to aerosol emission perturbations are investigated using NorESM (Bentsen

122 et al., 2013). This model is based on the Community Climate System Model 4.0 (CCSM4.0), but has been modified to include

123 interactive aerosols and to use the Bergen version of the Miami Isopycnic Coordinate Ocean Model (MICOM) instead of the

124 Parallel Ocean Program (POP) model. For NorESM the atmospheric component of the model, the Community Atmospheric

125 Model version 4 (CAM4) has been extended with an interactive aerosol module, CAM4-Oslo (Kirkevåg et al., 2013). The land

126 surface is represented by the Community Land Model version 4 (CLM4) and sea-ice is modelled with the ice model CICE4.

127 The atmospheric model uses a finite volume grid with a resolution of 1.9°x2.5° latitude-longitude.

128   The aerosol module in NorESM considers five different aerosol components: sulphate, black carbon, organic matter, min-

129 eral dust and sea salt. Both the mass and number for these aerosol constituents are predicted in a combined sectional and

130 modal framework. Emissions take place both in the form of primary particles and as precursors to aerosols where the aerosol

131 chemical compounds are produced through aqueous and gas phase chemical reactions. Aerosols can exist both as external

132 and internal mixtures, depending on atmospheric processing. E.g. sulphate coating of black carbon, which changes the optical

133 and hygroscopic properties of this internally mixed aerosol compared with the externally mixed constituents, is accounted for.

134 Humidification of aerosols is based on the hygroscopicity of the aerosol and the atmospheric relative humidity. Aerosols are

135 removed from the atmosphere by dry and wet deposition.

136   Aerosol can affect cloud properties through acting as cloud condensation nuclei (CCN). The efficiency of a particular aerosol

137 depends on its hygroscopicity and size. The amount of aerosol particles that are efficient CCN is connected to the predicted

138 aerosol size and mass and connected to the two-moment cloud microphysics for stratiform clouds in the model. Thus, NorESM

139 simulates both the cloud albedo effect and cloud lifetime effects of aerosols. Beside these effects of aerosols on cloud mi-

140 crophysical properties, semidirect effects which depend on changes of the thermal structure of the atmosphere are accounted

141 for.

142   An evaluation of the performance of NorESM in simulating the present climate was carried out by Bentsen et al. (2013),

143 who identified the main biases in the modelled climate compared to observations and that the model simulates a stable climate.

144 Iversen et al. (2013) derived climate sensitivities for NorESM and investigated the climate response to different future emission

Atmospheric
Chemistry
and Physics
Discussions

Open Access

145 scenarios. They found that the CO_2 climate sensitivity of the model is smaller than the Coupled Model Intercomparison Project

146 phase 5 (CMIP5) multi-model mean, but within one standard deviation.

2.3 Experiments

148 We perform a suite of model simulations with NorESM where aerosol precursor emissions are perturbed in one region at a

149 time. Four regions which we consider being of particular interest from an aerosol and air-pollution perspective are studied:

150 Europe, North America, South Asia and East Asia. The emissions of anthropogenic aerosols have changed considerably in

151 these regions during the 20th century (e.g. Lamarque et al., 2010).

152 The emission regions (North America - NA, Europe - EU, South Asia - SA and East Asia - EA) are defined according

153 to the updated region definition of the Task Force on Hemispheric Transport of Air Pollution (HTAP), see Fig. 1, and the

154 aerosol emissions are the historical emissions of CMIP5 described by Lamarque et al. (2010). The aerosol type we study here

155 is ammonium sulphates and thus we perturb the anthropogenic sulphur dioxide (SO_2) emissions provided for CMIP5.

156 Year 2000 is chosen as the baseline year and aerosol emissions, aerosol precursor emissions, trace gas concentrations and

157 land use representing this year are used for the control simulation. In the emission perturbation experiments, the anthropogenic

158 aerosol precursor emissions are decreased or increased compared to year 2000 emissions and kept constant in each region

159 throughout the simulation. In total five coupled sensitivity experiments were performed, four experiments where SO_2 emissions

160 were increased in the four different regions and one where anthropogenic SO_2 emissions were removed over Europe. The

161 simulations were started from year 2000 in the transient historical CMIP5 simulation. The simulation length is 160 years for

162 simulations where emissions are increased. For the experiment where emissions are decreased the simulation length is 200

163 years. All the results presented are annual mean quantities and the first 50 years of each simulations have been removed before

164 averaging.

165 The SO_2 emission changes in the emission perturbation experiments are shown in Fig. 2. In the 0xEU experiment the SO_2

166 emissions in Europe are not completely eliminated. There remains 4.66 $Tgyr^{-1}$ of volcanic emissions of SO_2 in Europe (from

167 Etna). The SO_2 emissions in the rest of the experiments were increased by varying amounts depending on the magnitude of

168 the regional emissions in the control simulation. This was done to obtain a global mean instantaneous radiative forcing of

169 approximately -0.45 Wm^{-2} in all these perturbation experiments. For South Asian emissions, which are low in the control

170 simulation (6.47 $Tgyr^{-1}$ in year 2000 compared with 24.53 $Tgyr^{-1}$ in East Asia) the emissions were increased by a factor

171 of ten. Similarly, for Europe, North America and East Asia, SO_2 emissions were increased by a factor of seven, five and five

172 respectively.

173 The 0xEU experiment is included so that the effect of emission perturbation magnitude can be investigated, i.e. the sensitivity

174 to a relatively small emission reduction compared to a relatively large emission increase. The emission perturbation magnitude

175 (and sign, i.e. reduction) could also be considered as a more likely future scenario.

176   With the resulting global temperature response field of each emission perturbation experiment, RTP coefficients, dT_r/dEm_e,

177   can be constructed relating emission changes in the predefined emission regions, e, to any response region, r, of choice. The

178   emission-based ARTP can be calculated from the absolute emission change:

$$ARTP_{r,e}^{EM} = \Delta Em_e \frac{dT_r}{dEm_e}. \tag{3}$$

179   In addition to the coupled experiments we perform simulations to evaluate the Instantaneous Radiative Forcing (RF) and

180   Effective Radiative Forcing (ERF) of the aerosol emission perturbations in the coupled experiments.

181   The RF is derived from fixed Sea Surface Temperatures (SSTs) simulations where dual calls are made to the radiation code:

182   one call with climatological aerosols and another call where the emission perturbation aerosol concentrations and their effect

183   on cloud albedo are sent to the radiation code solely for diagnosing the radiative effect of these. Thus the meteorology in the

184   RF simulations is identical since the radiative effects of the emission perturbations do not feedback on the meteorology. With

185   this methodology the radiative effects alone from the aerosol can be quantified, without influence of fast or slow feedbacks.

186   The RF simulations are 7 years long and the 5 last years are used for the analysis.

187   The ERF is derived by performing fixed SST simulations with aerosol emission perturbations and letting the radiation

188   changes affect the meteorology. Thus, in addition to the aerosol direct radiative effect and cloud albedo effect the ERF also

189   includes radiative changes from fast feedbacks such as cloud microphysical and semidirect effects. In NorESM these effects

190   includes e.g. cloud liquid water content cloud fraction. These simulations are 20 years and the 15 last years are used for the

191   analysis.

192   In a simplified manner, the process chain from emission to global mean temperature response can be thought of a translation

193   of emission to column burden, to the instantaneous direct and indirect radiative forcing, to forcing including fast feedbacks, to

194   the full coupled temperature response. In an attempt to identify where the largest divergence appears in the process chain from

195   emission to temperature response in the experiments conducted with NorESM, we investigate the usefulness and accuracy of

196   alternative quantities to the unit emission in predicting the surface temperature response.

3   Results

3.1   Global forcing and temperature response

199   The simplest way to describe the sulphur emission perturbation impact on global and regional temperatures is to express

200   the temperature response in terms of temperature change per unit emission of sulphur (cf. Sect. 2.1). We first analyse the

201   results from the sensitivity experiments where SO_2 emissions were increased. The results from the 0xEU experiment will be

202   discussed in Sect. 3.3. The global mean temperature response per unit emission for these sensitivity experiments where the

203   SO_2 emissions were increased by comparable magnitudes the global temperature change per unit emission is similar within

204   10%. The temperature response varies from -0.0056 to -0.0061 $K(TgSyr^{-1})^{-1}$, depending on the location and magnitude of

205   the sulphur emission change (Table 2).

Atmospheric
Chemistry
and Physics
Discussions

Open Access

EGU

206   All global mean temperature changes are significantly different compared to the temperature of the year 2000 control simu-
207   lation, but are not significantly different between each other (Fig. 3a). Thus, the location of an emission change does not appear
208   to be a governing factor for the global mean temperature response modelled by NorESM. However, all emission changes are
209   located in the northern hemisphere, and atmospheric transport of aerosol particles will contribute to a redistribution of atmo-
210   spheric concentrations and the resulting column burden and radiative forcing of the aerosol, so that in some cases the resulting
211   column burden and radiative forcing from emission changes in different regions will partly overlap.

212   The global average RF per unit emission change (Table 2) shows larger variability than the global temperature response
213   (varying from -0.010 to -0.017 $Wm^{-2}(TgSyr^{-1})^{-1}$, the largest RF value being 62% larger than the smallest value), a larger
214   emission change is needed in EU than in SA to obtain the same RF change. The variability for the global mean ERF is similar
215   to that of the RF (difference of 64% between the largest and smallest value, varying from -0.008 to -0.026 $Wm^{-2}(TgSyr^{-1})^{-1}$)
216   but the magnitude of the global mean ERF is smaller than the RF for all emission-increase experiments except for the 5xNA
217   experiment. Thus, on a global scale, fast cloud feedbacks contribute to dampen the forcing effect of the emission increases in
218   NorESM.

3.1.1   Emission changes as predictor of global mean temperature change

220   As outlined in Sect. 2, the extreme simplification inherent in the method of describing the temperature response in terms of
221   emission perturbations, leads to uncertainties related to the generality of the RTP coefficients.

222   Figure 4a illustrates how SO_2 emission perturbations in the different experiments translate to global sulphate column burden,
223   RF, ERF and temperature anomalies. All values are normalised by the response in the North American experiments to illustrate
224   the relative amount of variability for each response quantity (i.e. response in the 5xNA experiment is always one in Figure 4.)

225   As noted previously, the global temperature responses per unit emission in the experiments where SO_2 emissions are in-
226   creased are not significantly different from each other. However, the translation from emission to column burden shows a
227   different pattern. For this quantity, the column burden per unit emission in the 10xSA experiment is 76% higher than in the
228   other experiments. Thus, the geographical location seems to be one factor controlling the column burden sensitivity to emis-
229   sion perturbations in the experiments where emissions are increased. The increased emissions in SA together with a local SA
230   reduction in precipitation of 0.22 $mmday^{-1}$ lead to a longer residence time of sulphate (0.73 days longer) as well as other
231   aerosol particles in NorESM in the 10xSA experiment compared to the control experiment.

232   A similar pattern as the column burden is evident for the normalised instantaneous RF response to a unit emission change.
233   The RF response to a unit emission change in SA is larger than the responses in the other experiments. Thus, there appears
234   to be a close connection between changes in the global sulphate column burden and the RF (correlation coefficient r=-0.985).
235   The normalised ERF sensitivity to unit emission perturbations, shows a larger variability between the experiments compared to
236   the other investigated quantities. The standard deviations for the global average ERF responses are also larger than that for RF.
237   This result indicates that cloud feedbacks, such as changes in liquid water content or cloud fraction and cloud albedo contribute
238   substantially to the ERF (cf. Table S1 in supplementary material), and also contributes to larger variability.

Atmospheric
Chemistry
and Physics
Discussions

239   Figure 4b shows the temperature response normalised by the different "basis quantities" (i.e. the leftmost group of bars in

240   Fig. 4b are identical to the rightmost bars in Fig. 4a). The perfect basis quantity would be one for which the heights of all

241   bars corresponding to the different experiments are equal. A basis quantity with this property would be the ideal predictor

242   of the global mean temperature response. Figure 4b shows that emission perturbation is a good predictor of the temperature

243   response for emission increases from all regions investigated when emissions are increased in all regions (standard deviations

244   corresponding the each group of bars are presented in Table 3). Instantaneous RF and column burden as basis quantities

245   underestimate the temperature response to SA emissions (this is connected to the larger column burden and RF sensitivity

246   to a unit emission perturbation in SA which do not translate to a larger temperature sensitivity). For ERF there is substantial

247   variability in the predictability for the temperature responses in the emission increase experiments, which also yields the largest

248   standard deviation of the basis quantities for these experiments. Thus, emission is a better predictor than the ERF of the global

249   temperature response for these emission increase experiments.

250   **3.2   Sub-global forcing and temperature response**

251   **3.2.1   Latitudinal forcing and temperature response**

252   The sub-global normalised temperature responses in the experiments where SO_2 emissions were increased display more varia-

253   tion between the different experiments than the global mean sensitivities. (As mentioned before, the 0xEU experiment will be

254   discussed in Sect. 3.3.2.) The latitudinal temperature responses per unit emission in the experiments with increased emissions

255   show a qualitatively similar pattern of increasing sensitivity with increasing latitude (Fig. 5). This pattern of Arctic amplifi-

256   cation is not dependent on the location of the emission perturbation in these experiments, neither in the latitudinal nor the

257   longitudinal direction. The temperature responses in each latitude band are significantly different from the temperature in the

258   year 2000 control simulation (at the 99% confidence level), except for the southern hemisphere temperature responses (indi-

259   cated by gray shading of the columns in Fig. 5). The latitudinal temperature responses in the different experiments are not

260   significantly different from each other, with the exception of most of the latitudinal temperature responses to SA emissions (at

261   the 90% confidence level, see Fig. 3 for details). Thus, the latitudinal temperature responses are in principle indistinguishable

262   for emission increases from EU, NA and EA, while the SA emission response is generally weaker.

263   The only latitudinal RF and ERF that are statistically significant are the responses to emissions increases in EU, NA and

264   EA, in NHml, the latitudinal band inside which these emission regions are located. Significant ERF responses are also found

265   in ARCT for the same emission source regions, but the ERF is larger in NHml where the emissions changes are located,

266   than in ARCT. SO_2 emissions increases in SA do not lead to any latitudinal average RF or ERF response that are statistically

267   significant. A large fraction of the atmospheric sulphur mass from SA emissions (which are mainly emitted in the Tropics)

268   is transported to the NHml region, so that the average RF, ERF and column burden in this region exceeds that of the tropical

269   region. However, the total integrated sulphur column burden is larger in the Tropics than in the NHml (not shown) in the 10xSA

270   experiment.

Atmospheric
Chemistry
and Physics
Discussions

271   The ERF acts to enhance the forcing relative to the RF in the NHml in all experiments, as well as in the ARCT region.

272   This is a manifestation of aerosol indirect effects which lead to e.g. higher cloud water content (Table S1). The ERF displays a

273   warming effect in the SHext in all experiments (due to decreases in low cloud fraction at southern hemisphere midlatitudes, not

274   shown), although this positive ERF is not significant in any experiment. However, the positive ERF in the southern hemisphere,

275   which represents a large part of the global mean, contributes to the lower value of global average of the ERF compared to the

276   RF (cf. Sect. 3.1).

277   As described above, the temperature responses in the latitudinal bands are similar between the experiments with the excep-

278   tion of the temperature responses to changed SO_2 emissions in SA. SA has the largest tropical response which, however, is only

279   significantly different from the tropical response to EU emissions, which is the weakest tropical response among the experi-

280   ments. Similarly, the ARCT response to SA emissions is the smallest among the experiments, and is only significantly different

281   to the ARCT response to NA emissions, which leads to the strongest response in ARCT. The weaker NHml response to SA

282   emissions compared to the other emission regions, on the other hand, is significantly different compared to all other NHml

283   temperature responses. The NA, EU and EA emission regions are to the greater part located in the northern hemisphere mid-

284   latitudes, and mostly north of the SA emission region. Thus, the longitudinal position of a mid-latitude emission perturbation

285   does not appear to matter for the latitude mean temperature responses at northern hemisphere high- and mid-latitudes.

286   **3.2.2   Regional temperature response**

287   The differences between the sub-global temperature responses in the different experiments become more evident when they

288   are derived for the emission perturbation regions (and the AR region north of 66°N) compared to when derived for latitudinal

289   bands (Fig. 7). All regional temperature changes are statistically significant compared to the control simulation. The largest

290   temperature response is found in the AR region in all experiments, which is consistent with the latitudinal distribution of

291   the temperature response for latitude bands described in the previous section. Similarly, the SA emissions have the smallest

292   effect on the AR temperature among the experiments, but the AR temperature response in this experiment is only significantly

293   different from the response to NA emissions, which give the largest AR response among the experiments.

294   Outside the AR region, the largest temperature response is found locally in the emission region in all experiments except

295   10xSA. This result is consistent with the forcing always being largest in the emission region (Fig. 8). The regional RF and ERF

296   is also statistically significant for local SO_2 emissions from SA, as opposed to when derived for the Tropical latitudinal band

297   (Fig. 6). For SA emissions the temperature response in the EA region is marginally larger than the local temperature response

298   in the SA region. The EA region is located downwind of the SA region, which means that a substantial part of the sulphur

299   emitted in SA is transported to EA and contribute to the local forcing in EA. The column burden increase by $3\%/TgSyr^{-1}$ in

300   EA due to SA emission, to be compared with the increase in EA due to local emission of $4\%/TgSyr^{-1}$. Additionally, advection

301   of air originating from SA might also partly explain the large temperature response in the EA region to SA emissions. EA is the

302   only region where there are emissions from a remote region (SA) that lead to a temperature response that is indistinguishable

303   from the effect of local emissions.

Atmospheric
Chemistry
and Physics
Discussions

304   The local temperature responses in the emission perturbation regions are larger than the corresponding zonal mean temper-

305   ature responses of the latitudes covered by each region (indicated by black dots in Fig. 7) in all experiments. The largest local

306   response relative to the zonal mean is found in the 10xSA experiment, which is 66% larger than the zonal mean. The 5xNA

307   experiment shows the largest absolute difference between the local response and the zonal mean, 0.0055 K/TgSyr^{-1} (55%

308   larger). The smallest local temperature response relative the zonal mean is found for 7xEU (20%). All differences between

309   these local responses and the corresponding zonal means are statistically significant at the 95% confidence level.

310   For both NA and EU emission perturbations, the temperature responses in the regions outside the emission regions are close

311   to the corresponding zonal mean responses (within 2-17% difference). SA and EA emission perturbations, on the other hand,

312   both lead to a larger temperature response than the corresponding zonal mean for NA and a smaller temperature response than

313   the zonal mean for EU, where both these differences between the zonal mean and regional temperature response are statistically

314   significant. Both EA and SA emission perturbations have a substantial effect on NA temperature, of the same magnitude as the

315   local responses for these emission regions, despite the geographical distance between the emission location and the temperature

316   response regions. Local radiative forcing in NA is not responsible for this temperature effect (Fig. 8). This result points towards

317   a far field effect in the temperature response to Asian aerosol forcing which is mediated by atmospheric circulation changes

318   rather than radiation changes.

3.3   Nonlinearities

320   So far, only the results from the experiments where SO$_2$ emissions were increased have been discussed. In this section we will

321   focus on the differences between the results from the 0xEU and 7xEU SO$_2$ emission changes experiments. The purpose is to

322   investigate if the emission perturbation magnitude or background state influences the temperature response (cf. e.g. Wilcox

323   et al., 2015).

3.3.1   Global temperature response

325   In the experiment where European anthropogenic SO$_2$ emissions are removed, the global average temperature change per unit

326   emission is approximately twice of that in the 7xEU experiment, as well as in the other experiments where emissions were

327   increased (Fig. 4 and Table 2). This indicates that there is a non-linearity depending on the magnitude and sign of the emission

328   change, at least for European SO$_2$ emissions. Since the coupled simulations include aerosol indirect effects, and since indirect

329   effects are usually larger than direct aerosol effects (Rap et al., 2013; Myhre et al., 2013; Kirkevåg et al., 2013), nonlinear

330   effects pertaining to aerosol-cloud interactions most likely play a role in the difference in global climate sensitivity between

331   the 0xEU and 7xEU experiments. However, effects related to the modeled aerosol microphysics could also play a role in this

332   difference, in particular when SO$_2$ emissions and concentrations are low. E.g. in extreme conditions the partitioning between

333   different aerosol microphysical paths might change, like condensation and nucleation rates of sulphate (Stier et al., 2006).

334   The two experiments with different European SO$_2$ emission perturbations illustrate the difficulties related to the generality

335   of the method of translating emission perturbations to temperature response already discussed in Section 3.1. The global mean

temperature responses per unit sulphur emission differ substantially for these two experiments, as well as the magnitudes of the latitudinal and regional temperature responses.

We return to the question of "basis quantities" (cf. Sect. 3.1) and for which step in the translation from emission to temperature response the largest divergence appears for the different experiments. The normalised global temperature responses per unit emission in the experiments where SO_2 emissions are increased are close to unity, while the normalised temperature response per unit emission in the 0xEU experiment is larger than two (Fig. 4). The translation from emission to column burden for the EU emission changes is not dependent on the emission magnitude in the experiments presented here. Similar to what was noted for the other experiments, the RF per unit emission change in 0xEU and 7xEU is similar to the column burden response per unit emission change. The normalised ERF sensitivity to unit emission perturbation on the other hand, bears more resemblance with the temperature response for the 0xEU and 7xEU experiments (third group of bars/the next rightmost bars in Fig. 4a). This indicates that fast cloud feedbacks, such as cloud lifetime, liquid water content or semidirect effects, is most likely a key component for understanding the non-linearity in the temperature response to European emissions (cf. Table S1 and S2).

Emission perturbation was in Sect. 3.1 found to be a a good predictor of the temperature response for emission increases from all regions investigated when the emissions were increased with similar magnitudes. However, it does not capture the non-linear behaviour in the temperature response to European emission perturbations of different magnitudes (Fig. 4b). Similarly, RF and column burden as basis quantities also fail to capture this property in the response to European emission perturbations. The ERF is the only basis quantity that captures the non-linearity for European emission perturbations of varying magnitude. However, there is substantial variability in the predictability for the temperature responses in the other experiments. The ERF shows the smallest standard deviation for the different basis quantities when all experiments are considered (Table 3), but this is due to substantially larger standard deviations for emissions, CB and RF as basis quantities when the 0xEU experiment is included. Nevertheless, the ERF is the basis quantity with the highest degree of generality for the global results from all the experiments conducted with NorESM presented in this study.

3.3.2 Sub-global temperature response

Similarly to the global mean response, the magnitude of the latitudinal and regional temperature responses per unit sulphur emission are substantially larger in the 0xEU experiment than in the 7xEU experiment, with the exception for the temperature difference in SA which is not statistically significant compared to the control simulation (Fig. 9, where that hatched bars indicate the 7xEU response for easy comparison). For the latitudinal sensitivities, the pattern of increasing temperature response with latitude found in the experiments where emissions were increased (Sect. 3.2.1 and Fig. 5) is also seen for the 0xEU experiment. The relative impact on the southern hemisphere is also larger in this experiment compared to the other experiments. All latitudinal temperature changes in the 0xEU experiment are significantly different from the responses in all the other experiments except for the tropical latitude band (Fig. 3).

The regional 0xEU responses display a similar pattern to the regional responses in the 7xEU experiment, but with different magnitudes. The largest temperature response is seen in the AR region whereas outside AR the largest response is found in the

Atmospheric
Chemistry
and Physics
Discussions

370 emission region (EU). The temperature responses to reduced EU SO$_2$ emissions in NA and EA are close to the zonal means

371 for the latitudes covered by these regions (within 2%). This is similar to the the corresponding regional temperature responses

372 in the 7xEU experiment relative to the zonal mean responses.

373 The non-linear effects are mostly confined to the magnitude of the temperature responses in the case for European emission

374 perturbations in these experiments. Zonal asymmetries do not appear to have a significant impact on the regional temperature

375 responses. This might, however, be different for the Asian emission perturbations where zonal asymmetries seem to play a more

376 prominent role in the regional temperature distributions compared to the European and North American emission perturbations.

3.4 Comparison with other RTP coefficients

378 In this work we have aimed to establish the simplest possible model for anthropogenic aerosol impacts on regional tempera-

379 tures, i.e. an emission-based regional temperature potential coefficient.

380 Nevertheless, difficulties associated with nonlinear effects in this relationship remain where ERF proved to be a more general

381 basis quantity for estimating the global temperature response than emissions, in terms of capturing different magnitudes of

382 global mean temperature responses for different emission changes in Europe.

383 With the experimental set up applied in this study, it is not possible to derive sub-global (latitudinal or regional) radia-

384 tive forcing-based sensitivities, as the forcing changes in the different experiments are not confined to a certain region or

385 latitude band. However, with the latitudinal and regional RF and ERF from the different experiments, the generality of the

386 RTP-coefficients derived by Shindell and Faluvegi (2009) and Shindell (2012) can be assessed for the NorESM generated

387 temperature response. For each experiment the RF and ERF in each latitude band resulting from the regional emission per-

388 turbations are calculated (Table 4) and used with different methods for calculating the latitudinal temperature responses, the

389 ARTP.

390 First we compare the temperature response as calculated from Equations 1 and 2 with that from the simulations with NorESM

391 where SO$_2$ emissions were increased. Both equations require knowledge of the model global climate sensitivity (or the Impulse

392 Response Function). The climate sensitivities are derived from the emission perturbation experiments, and we use a mean value

393 from all experiments with emission increases. Climate sensitivities for both RF and ERF are derived, and these are calculated

394 to be 0.47 and 0.61 K(Wm^{-2})$^{-1}$, respectively.

395 However, the model global climate sensitivity is not always known, e.g. if the forcing is derived with a Chemistry Trans-

396 port Model (CTM). Moreover, one motivation behind using RTP coefficients is to avoid conducting multi-century coupled

397 simulation, which is necessary for deriving the climate sensitivity. Therefore, we also evaluate the performance of the RTP

398 coefficients with a standardised climate sensitivity as well as applying the RTP coefficients of Shindell and Faluvegi (2010)

399 as regional sensitivity coefficients (i.e. without normalising with the regional climate sensitivity to global forcing and scaling

400 with the models global sensitivity). This is to see how well the RTP-method predicts the model temperature response when the

401 specific model's climate sensitivity to a particular forcing agent is unknown.

402 The latitudinal temperature responses calculated from Equations 1 and 2 are shown in Fig. 10 and 11. The small dots indicate

403 the temperature response in specific regions and the filled circles indicate the emission source regions. The high latitude

Atmospheric
Chemistry
and Physics
Discussions

404 temperature response in the northern hemisphere (ARCT) calculated using the RTP coefficients, the ARTP, is underestimated

405 compared to the temperature response in the NorESM experiments (but still within one standard deviation of the NorESM

406 simulated temperature response), except for when the ERF is used in combination with the normalised coefficients of Shindell

407 et al. (2012) (Fig. 11b). This is also the method that gives the smallest root mean square deviation (RMSD) of 0.14K (RMSDs

408 are displayed in each panel). In general, ERF is a better predictor of the latitudinal temperature response than RF, based on

409 the RMSD. Similarly, the RTP coefficients that are normalised by the global sensitivity (Shindell et al., 2012) rather that the

410 regional sensitivity (Shindell and Faluvegi, 2010), i.e. Fig. 10 vs. Fig. 11, is a better model for the temperature response in each

411 latitude band, also based on the RMSD. This was also pointed out by Shindell (2012).

412   However, the performance of this method relies on that the correct climate sensitivity is used and is known. The standard

413 definition of equilibrium climate sensitivity (ECS) is the equilibrium temperature response to a doubling of CO_2 (Collins et al.,

414 2013), and is available for nearly all models participating in the Coupled Model Intercomparison Project phase 5 (Flato et al.,

415 2013). For NorESM this climate sensitivity has been estimated to 1.01 $Wm^{-2}K^{-1}$ (Iversen et al., 2013). This is higher than

416 the sensitivity to aerosol forcing obtained in this study. The results of the RTP method with this ECS applied is shown in Figure

417 12. Overall, the use of ECS overestimates the temperature response in almost all latitude bands. Thus, it is important to use the

418 correct climate sensitivity for the climate forcer investigated. This is a complicating factor since it requires a priori knowledge

419 of this quantity, which can only be derived by performing coupled simulations, the necessity of which one often would like

420 to eliminate with a simplified method. Moreover, if calculations to derive radiative forcing are performed with a CTM, this

421 quantity is not available.

422   A third alternative is to apply the RTP coefficients without normalising with a model dependent climate sensitivity parameter

423 (Fig. 13). The implicit assumption in this method is that the sensitivity of NorESM to aerosol forcing is equal to that of the

424 GISS model in Equation 2, a transient sensitivity of 0.5 K/Wm^{-2} (Shindell, 2012). This assumption about the sensitivity leads

425 to RTP-derived temperature responses with smaller RMSD values than both those derived by applying the ECS for NorESM

426 in Equation 1 and 2.

427   Figure 13 shows that assuming that the sulphate aerosol climate sensitivity is similar between different climate models might

428 be better than assuming that the climate sensitivity for sulphate aerosol is similar to the ECS derived from the same model.

4 Discussion

4.1 Uncertainties associated with RTP coefficients

431 The method applied in this work, i.e. evaluating the global and regional temperature responses based on the emission change

432 magnitudes, means that on the one hand, the starting quantity is easy to assess and compare and is easy to incorporate into

433 integrated assessment models, such as GAINS. The full response chain from emissions to atmospheric concentrations, to forc-

434 ing, to surface temperature response is accounted for in this metric. On the other hand, the fact that the metric encompasses

435 the full chain from emission to temperature response means that there are implicit uncertainties in the metric. The representa-

436 tiveness of these emission based RTP coefficients will depend on how well the climate model used to derive these coefficients,

437 represents a large number of atmospheric chemical and physical processes on many different spatial and temporal scales. The

438 RTP coefficients derived by Shindell and Faluvegi (2009) and Shindell (2012) were derived from radiative forcing, and thus

439 do not contain the uncertainties introduced when estimating the column burden and forcing associated with aerosol emissions.

440 However, a model to translate emission to radiative forcing, either RF or ERF, is still necessary to make these forcing based

441 RTP coefficients useful in an integrated assessment modelling context based on emission pathways.

442 Some major uncertainties can be identified if the emission-temperature response chain is broken down into sub steps. First,

443 emissions of an atmospheric chemical compound result in an atmospheric concentration and column burden. The translation

444 from emission of an atmospheric chemical component to atmospheric aerosol loading depends on a number of factors, e.g. if the

445 aerosol originates from primary emission or is formed through chemical reactions in the atmosphere (i.e. secondary aerosols),

446 like sulphate which is studied here. The aerosol production for secondary aerosols will depend on which and how chemical

447 reactions that produce these aerosols are described in the atmospheric model. Kasoar et al. (2016) found that the efficiency of

448 chemical conversion of SO_2 to sulphate was one process contributing to differences in the simulated responses in three different

449 climate models to equivalent emission reductions over China. In addition to chemical production, the interaction with clouds

450 will influence the atmospheric concentration of aerosols. Wet removal through precipitation is an efficient removal process

451 for hygroscopic aerosols like sulphate containing compounds. All these factors, emission strength, atmospheric production

452 and removal efficiency influence how long aerosol particles stay in the atmosphere and how far they are transported from the

453 emission sources. Thus, all these processes influence the atmospheric loading and how these processes are represented in the

454 model will influence the modelled aerosol column burden.

455 Another source of uncertainty in the emission-forcing-temperature chain, besides the modelled column burden, is how the

456 aerosol radiative properties are modelled (Myhre et al., 2013). The radiative properties of aerosols depend on e.g. their chemical

457 composition, water content and mixing state. Thus, given the same atmospheric concentration and distribution of aerosols, their

458 radiative effect might vary depending on how their radiative properties are represented in the model. Other complicating factors

459 when it comes to aerosol radiative effects are clouds and aerosol indirect and semi-direct effects on clouds. The direct radiative

460 forcing will depend on the cloud distribution itself, and aerosol can affect the properties of clouds and also, affect the cloud

461 distribution, i.e. other components, besides the aerosol itself, within the model influence their radiative effects (Stier et al.,

462 2013).

463 One of the largest uncertainties associated with the effect of aerosols on climate is related to their indirect effect on clouds

464 (Myhre et al., 2013) and the representation of these can vary widely between different models. Beside chemical conversion

465 and radiative impacts, Kasoar et al. (2016) also identified indirect effects on clouds as a major source of diversity between the

466 models they investigated. Wilcox et al. (2015) found that parameterisations of the relationship between cloud droplet number

467 concentration and effective radius was the largest contribution to differences in the cloud albedo effect between three models

468 from the CMIP5 archive, among those NorESM.

469 The factors described above all contribute to inter-model diversity, and will influence how general RTP coefficients are

470 across models. However, the same processes also contribute to regional sensitivity differences within the same model, but not

Atmospheric
Chemistry
and Physics
Discussions

Open Access

EGU

471 based on differences in how the processes are represented in the model, but on the specific meteorological conditions in each

472 region (e.g. cloud climatology, regional circulation patterns and the background aerosol).

473   It is evident from the results presented in this study that the temperature sensitivity depends on the emission change magni-

474 tude in NorESM. The nonlinearity in the response appears to belong to aerosol interactions with clouds and in particular to fast

475 feedbacks included in the ERF. These include changes in liquid water content, cloud fraction and subsequent changes in cloud

476 albedo of the new cloud distribution, i.e. cloud life time effects (Albrecht, 1989) (the cloud albedo effect of the background

477 cloud distribution is included in RF).

478   Wilcox et al. (2015) derived simple functional forms representing the relationship between sulphate load and cloud droplet

479 effective radius (i.e. the cloud albedo effect) in three different CMIP5 models, with which they could reproduce the time

480 evolution of the simulated cloud droplet effective radius from historical 20th century simulations. With these functional forms,

481 they could also quantify the intrinsic varying sensitivity in the parameterisation of the effective radius which depends on the

482 magnitude of the sulphate load, and how the effective radius (and ultimately radiative forcing) goes from being highly sensitive

483 at low sulphate loads to a relative insensitive state at high sulphate loads. While they focussed on the cloud albedo effect, the

484 cloud life time effect is a direct consequence of initial change in effective radius, and should thus display a similar varying

485 sensitivity depending on the absolute sulphate load.

486   Thus, the similarity of the global temperature responses in the emission increase experiments, despite different mechanisms,

487 might be due to this saturation of cloud droplet effective radius change when emission increases are large enough. The tem-

488 perature sensitivity for the different regions could prove to be different if emission were reduced, even by equivalent amounts,

489 depending on the regional background emission strength and regional meteorological conditions. Nonlinear effects depending

490 on the emission change magnitude and background is one of the biggest hurdles in creating a general emission based RTP

491 coefficient.

492 **4.2   Basis quantity**

493 Different quantities for predicting the temperature response have been assessed for the global mean temperature and for latitu-

494 dinal bands in combination with the RTP coefficients of Shindell and Faluvegi (2010) and Shindell (2012). In both cases ERF

495 proved to have the best skills to predict the temperature response.

496   For the global mean temperature response, the ERF was the only variable that was capable of capturing the large difference

497 in the temperature responses to the European increase and decrease in SO_2 emissions. However, for the emission increase

498 experiments, emission was the quantity that best predicted the temperature change. Also for the latitudinal ARTPs the ERF

499 performed better in predicting temperature responses than the RF for NorESM, which is mostly due to a simulated larger ERF

500 than RF in the Arctic region. This can either be an indication that the sensitivity of the Arctic region is larger in NorESM than

501 GISS to forcing outside the Arctic region, i.e. that the coefficient relating the forcing to Arctic temperature responses should

502 be larger for NorESM. It could also be an indication that the cloud feedbacks in the Arctic is a necessary part of the forcing,

503 and that the local forcing from fast feedbacks is important for the Arctic response in NorESM.

4.3 Latitudinal and regional sensitivities

504

505 The sensitivity of zonal mean temperatures to emission perturbations in different regions show large similarities, with the

506 exception of the overall weaker northern hemisphere temperature response to SA SO_2 emissions; the zonal mean temperature

507 change increase with increasing latitude in all experiments and do not appear to depend strongly on the location of the emission

508 perturbations within the northern hemisphere (Fig. 5). There are many factors that might contribute to the weaker temperature

509 response to the SA emission perturbation. This emission perturbation is located in one of the major monsoonal regions on the

510 globe, and the increase of sulphate leads to a substantial reduction of precipitation over SA (Table S1 and S2). The reduced

511 precipitation, in turn, leads to less efficient wet removal of aerosol resulting in an increased residence time and a larger column

512 burden response per unit emission of both sulphate and BC compared to the control simulation. The decrease in precipitation

513 in SA (as well as smaller increases in liquid water path, Table S1 and S2) also contribute to a weaker ERF and indirect effect

514 on clouds, which, in the other experiments enhances the local forcing, but not in SA (Fig. 8). This result is one example of how

515 different local meteorological conditions where the emission changes occur contribute to different forcing and temperature

516 responses within the same model.

517 The general pattern, which indicates a stronger temperature response with increasing latitude for all emission perturbations,

518 is a robust feature in all experiments. In all experiments, the second largest regional sensitivity (after the Arctic region), is

519 generally found in the region of the emission perturbation. However, for SA emissions, the sensitivity is slightly larger in the

520 East Asian region compared to the South Asian emission region, a result caused by production of sulphate aerosol from SO_2

521 and subsequent transport from SA to EA.

522 Moreover, Asian SO_2 emissions, both from EA and SA, produce larger zonal asymmetries in the global temperature change

523 field than those of EU and NA. The Asian SO_2 emissions lead to temperature responses in NA and EU that are higher and

524 lower, respectively, than the zonal mean response. The remote regional temperature responses to EU and NA SO_2 emissions are

525 on the other hand close to the corresponding zonal mean responses. The location in the Asian monsoon region and proximity

526 to the Western Pacific mean that these SO_2 emissions could cause tropical precipitation changes that are effective in generat-

527 ing planetary scale waves. These waves can propagate into the extratropics, which in turn influences the global temperature

528 distribution (Ming et al., 2011; Lewinschal et al., 2013).

529 However, the standard deviations for the regional sensitivities are larger than those for the latitudinal sensitivities and zonal

530 mean sensitivities. Nevertheless, despite the larger uncertainties associated with the regional RTPs compared to the latitudinal

531 RTPs, they provide information that is not captured by the latitudinal RTPs.

5 Summary and Conclusions

532

533 We performed simulations with the Earth system model NorESM to evaluate the surface temperature change in response to

534 SO_2 emission perturbations in Europe, North America and East and South Asia, and to derive emission-based RTP coefficients.

535 Four experiments were performed where emissions were increased relative to the year 2000 in each individual region to yield

Atmospheric
Chemistry
and Physics
Discussions

536 similar global mean radiative forcing values. One additional experiment was performed where anthropogenic SO_2 emissions

537 were completely removed in Europe.

538 In all five experiments the zonal mean latitudinal temperature change distribution showed a similar pattern of increasing

539 temperature change with increasing latitude, independently of where the emission perturbation was located. The largest tem-

540 perature response in all experiments performed was in this study thus found in the Arctic region, no matter where the emission

541 perturbations were located. Outside the Arctic region, the temperature response was largest in the emission perturbation re-

542 gion, except for SA emissions where the temperature response in the neighbouring EA region was equally large. This result

543 was consistent with the radiative forcing pattern, which was also strongest in the emission region in each experiment.

544 Furthermore, it was found that the emission-based RTPs derived with NorESM are non-linear. Removal of anthropogenic

545 European SO_2 emissions led to a temperature response per unit emission approximately twice of that in the 7xEU experiment.

546 Other differences were also noticed for the regional responses to regional emission perturbations. Asian emission increases led

547 to a different remote effect compared to increases in EU and NA emissions. Both EA and SA emission perturbations led to

548 a NA temperature response that was larger than the zonal mean and an EU response that was smaller than the corresponding

549 zonal mean. EU and NA emission perturbations, on the other hand, led to remote responses that were close to the zonal mean

550 for the same latitudes.

551 A comparison of the modelled temperature response in NorESM with that calculated using ARTPs (equations 1 and 2)

552 derived with the RTP coefficients of Shindell and Faluvegi (2010) and Shindell (2012) showed that the RTP coefficients predict

553 similar latitudinal temperature change distributions as those produced by NorESM. The agreement between the calculated

554 values using ARTPs and the temperature change simulated using NorESM was better when ERF was used together with the

555 RTP coefficient than when RF was used. This was mainly due to a larger Arctic ERF than RF that resulted in an Arctic

556 temperature response closer to that produced in the NorESM simulations. This result could be an indication that the Arctic is

557 more sensitive to forcing outside this region in NorESM than in the GISS model, or that local fast cloud feedbacks are crucial

558 for the Arctic temperature response in NorESM.

559 Even though the global mean temperature response to emission increases is similar in all regions, the processes leading to

560 the change may be different in different regions, as it depends on the local meteorological conditions. In all regions except SA,

561 aerosol indirect effects on clouds, and particularly life time effects, are dominating the ERF response. For SA, direct radiative

562 effects have a higher relative importance in the response since the local responses in cloud fraction, liquid water path and

563 precipitation are either weaker compared to the other emission regions or decrease in response to increased SO_2 emissions.

564 The latitudinal distribution of the zonal mean temperature response to SA emission changes also differs from the rest of the

565 simulations in that the Northern hemisphere response is weaker and the southern hemisphere and tropical responses are stronger

566 than in the other simulations.

567 Air pollution globally cause more than 4 million premature deaths each year and as sulphates are major air pollution com-

568 ponents, emission reductions of SO_2 will be absolutely necessary to improve air quality. The derived emission-based RTPs

569 will simplify development of cost effective co-beneficial abatement strategies that can give both better air quality and mitigate

570 climate change. The nonlinear effect predicted by NorESM indicate a reduced immediate climate effect of SO_2 emission re-

571 ductions in highly polluted areas where the indirect effect is saturated but the effect would become more evident with time as

572 the saturation of aerosol indirect effects diminishes. Nevertheless, emission reductions of SO_2 and other short-lived climate

573 forcers are necessary for improving air quality and public health in both Europe, North America and Asia.

574 *Author contributions.* AL, AMLE, HCH, MS, TKB and JL designed the experiments. AL carried out the simulations. AL prepared the

575 manuscript with contributions from all co-authors.

576 *Competing interests.* The authors declare that they have no conflict of interest.

Atmospheric
Chemistry
and Physics
Discussions

References

581 Aamaas, B., Peters, G. P., and Fuglestvedt, J. S.: Simple emission metrics for climate impacts, Earth System Dynamics, 4, 145–170,
582   https://doi.org/10.5194/esd-4-145-2013, 2013.

583 Acosta Navarro, J. C., Varma, V., Riipinen, I., Seland, O., Kirkevag, A., Struthers, H., Iversen, T., Hansson, H. C., and Ekman, A. M. L.:
584   Amplification of Arctic warming by past air pollution reductions in Europe, Nature Geosci., 9, https://doi.org/10.1038/NGEO2673, 2016.

585 Albrecht,   B.:   Aerosols,   cloud   microphysics,   and   fractional   cloudiness,   Science,   245,   1227–1230,
586   https://doi.org/10.1126/science.245.4923.1227, 1989.

587 Amann, M., Bertok, I., Borken-Kleefeld, J., Cofala, J., Heyes, C., Hoeglund-Isaksson, L., Klimont, Z., Nguyen, B., Posch, M., Rafaj, P.,
588   Sandler, R., Schoepp, W., Wagner, F., and Winiwarter, W.: Cost-effective control of air quality and greenhouse gases in Europe: Modeling
589   and policy applications, Environmental Modelling & Software, 26, 1489–1501, https://doi.org/10.1016/j.envsoft.2011.07.012, 2011.

590 Bellouin, N., Baker, L., Hodnebrog, O., Olivie, D., Cherian, R., Macintosh, C., Samset, B., Esteve, A., Aamaas, B., Quaas, J., and Myhre, G.:
591   Regional and seasonal radiative forcing by perturbations to aerosol and ozone precursor emissions, Atmospheric Chemistry and Physics,
592   16, 13 885–13 910, https://doi.org/10.5194/acp-16-13885-2016, 2016.

593 Bentsen, M., Bethke, I., Debernard, J. B., Iversen, T., Kirkevag, A., Seland, O., Drange, H., Roelandt, C., Seierstad, I. A., Hoose, C., and
594   Kristjansson, J. E.: The Norwegian Earth System Model, NorESM1-M - Part 1: Description and basic evaluation of the physical climate,
595   Geoscientific Model Development, 6, 687–720, https://doi.org/10.5194/gmd-6-687-2013, 2013.

596 Collins, M., Knutti, R., Arblaster, J., Dufresne, J.-L., Fichefet, T., Friedlingstein, P., Gao, X., Gutowski, W., Johns, T., Krinner, G., Shongwe,
597   M., Tebaldi, C., Weaver, A., and Wehner, M.: Long-term Climate Change: Projections, Commitments and Irreversibility., In: Climate
598   Change 2013: The Physical Science Basis. Contribution of Working Group I to the Fifth Assessment Report of the Intergovernmental
599   Panel on Climate Change [Stocker, T.F., D. Qin, G.-K. Plattner, M. Tignor, S.K. Allen, J. Boschung, A. Nauels, Y. Xia, V. Bex and P.M.
600   Midgley (eds.)]. Cambridge University Press, Cambridge, United Kingdom and New York, NY, USA., 2013.

601 Dong, B., Sutton, R. T., Highwood, E. J., and Wilcox, L. J.: Preferred response of the East Asian summer monsoon to local and non-local
602   anthropogenic sulphur dioxide emissions, Climate Dynamics, 46, 1733–1751, https://doi.org/10.1007/s00382-015-2671-5, 2016.

603 Flato, G., Marotzke, J., Abiodun, B., Braconnot, P., Chou, S., Collins, W., Cox, P., Driouech, F., Emori, S., Eyring, V., Forest, C., Gleckler,
604   P., Guilyardi, E., Jakob, C., Kattsov, V., Reason, C., and Rummukainen, M.: Evaluation of Climate Models., In: Climate Change 2013:
605   The Physical Science Basis. Contribution of Working Group I to the Fifth Assess- ment Report of the Intergovernmental Panel on Climate
606   Change [Stocker, T.F., D. Qin, G.-K. Plattner, M. Tignor, S.K. Allen, J. Boschung, A. Nauels, Y. Xia, V. Bex and P.M. Midgley (eds.)].
607   Cambridge University Press, Cambridge, United Kingdom and New York, NY, USA., 2013.

608 Iversen, T., Bentsen, M., Bethke, I., Debernard, J. B., Kirkevag, A., Seland, O., Drange, H., Kristjansson, J. E., Medhaug, I., Sand, M., and
609   Seierstad, I. A.: The Norwegian Earth System Model, NorESM1-M - Part 2: Climate response and scenario projections, Geoscientific
610   Model Development, 6, 389–415, https://doi.org/10.5194/gmd-6-389-2013, 2013.

611 Kasoar, M., Voulgarakis, A., Lamarque, J.-F., Shindell, D., Bellouin, N., Collins, W., Faluvegi, G., and Tsigaridis, K.: Regional and global
612   temperature response to anthropogenic SO_2 emissions from China in three climate models, Atmospheric Chemistry and Physics, 16,
613   9785–9804, https://doi.org/10.5194/acp-16-9785-2016, http://dx.doi.org/10.5194/acp-16-9785-2016, 2016.

614 Kirkevåg, A., Iversen, T., Seland, O., Hoose, C., Kristjánsson, J. E., Struthers, H., Ekman, a. M. L., Ghan, S., Griesfeller, J., Nilsson, E. D.,
615   and Schulz, M.: Aerosol-climate interactions in the Norwegian Earth System Model - NorESM1-M, Geoscientific Model Development,
616   6, 207–244, https://doi.org/10.5194/gmd-6-207-2013, 2013.

Atmospheric
Chemistry
and Physics
Discussions

617 Lamarque, J.-F., Bond, T. C., Eyring, V., Granier, C., Heil, A., Klimont, Z., Lee, D., Liousse, C., Mieville, A., Owen, B., Schultz, M. G.,
618   Shindell, D., Smith, S. J., Stehfest, E., Aardenne, J. V., Cooper, O. R., Kainuma, M., Mahowald, N., McConnell, J. R., Naik, V., Riahi,
619   K., and van Vuuren, D. P.: Historical (1850-2000) gridded anthropogenic and biomass burning emissions of reactive gases and aerosols:
620   methodology and application, Atmospheric Chemistry and Physics, 10, 7017–7039, doi:10.1029/2007GL030541, 2010.

621 Lewinschal, A., Ekman, A. M. L., and Kornich, H.: The role of precipitation in aerosol-induced changes in northern hemisphere wintertime
622   stationary waves, Climate Dynamics, 41, 647–661, https://doi.org/10.1007/s00382-012-1622-7, 2013.

623 Menon, S., Hansen, J., Nazarenko, L., and Luo, Y.: Climate effects of black carbon aerosols in China and India, Science, 297, 2250–2253,
624   2002.

625 Ming, Y., Ramaswamy, V., and Chen, G.: A model investigation of aerosol-induced changes in boreal winter extratropical circulation, Journal
626   of Climate, 24, 6077–6091, doi: 10.1175/2011JCLI4111.1, 2011.

627 Myhre, G., Shindell, D., Bréon, F.-M., Collins, W., Fuglestvedt, J., Huang, J., Koch, D., Lamarque, J.-F., Lee, D., Mendoza, B., Nakajima,
628   T., Robock, A., Stephens, G., Takemura, T., and Zhang, H.: Anthropogenic and Natural Radiative Forcing., In: Climate Change 2013:
629   The Physical Science Basis. Contribution of Working Group I to the Fifth Assessment Report of the Intergovernmental Panel on Climate
630   Change [Stocker, T.F., D. Qin, G.-K. Plattner, M. Tignor, S.K. Allen, J. Boschung, A. Nauels, Y. Xia, V. Bex and P.M. Midgley (eds.)].
631   Cambridge University Press, Cambridge, United Kingdom and New York, NY, USA, 2013.

632 Myhre, G., Samset, B. H., Schulz, M., Balkanski, Y., Bauer, S., Berntsen, T. K., Bian, H., Bellouin, N., Chin, M., Diehl, T., Easter, R. C.,
633   Feichter, J., Ghan, S. J., Hauglustaine, D., Iversen, T., Kinne, S., Kirkevag, A., Lamarque, J. F., Lin, G., Liu, X., Lund, M. T., Luo, G.,
634   Ma, X., van Noije, T., Penner, J. E., Rasch, P. J., Ruiz, A., Seland, O., Skeie, R. B., Stier, P., Takemura, T., Tsigaridis, K., Wang, P., Wang,
635   Z., Xu, L., Yu, H., Yu, F., Yoon, J. H., Zhang, K., Zhang, H., and Zhou, C.: Radiative forcing of the direct aerosol effect from AeroCom
636   Phase II simulations, Atmospheric Chemistry and Physics, 13, 1853–1877, https://doi.org/10.5194/acp-13-1853-2013, 2013.

637 Rap, A., Scott, C. E., Spracklen, D. V., Bellouin, N., Forster, P. M., Carslaw, K. S., Schmidt, A., and Mann, G.: Natural aerosol direct and
638   indirect radiative effects, Geophysical Research Letters, 40, 3297–3301, https://doi.org/10.1002/grl.50441, 2013.

639 Shindell, D. and Faluvegi, G.: Climate response to regional radiative forcing during the twentieth century, Nature Geoscience, 2, 294–300,
640   https://doi.org/10.1038/NGEO473, 2009.

641 Shindell, D. and Faluvegi, G.: The net climate impact of coal-fired power plant emissions, Atmospheric Chemistry and Physics, 10, 3247–
642   3260, 2010.

643 Shindell, D., Schulz, M., Ming, Y., Takemura, T., Faluvegi, G., and Ramaswamy, V.: Spatial scales of climate response to inhomogeneous
644   radiative forcing, Journal of Geophysical Research-Atmospheres, 115, https://doi.org/10.1029/2010JD014108, 2010.

645 Shindell, D. T.: Evaluation of the absolute regional temperature potential, Atmospheric Chemistry and Physics, 12, 7955–7960,
646   https://doi.org/10.5194/acp-12-7955-2012, 2012.

647 Shindell, D. T., Lamarque, J.-F., Schulz, M., Flanner, M., Jiao, C., Chin, M., Young, P., Lee, Y. H., Rotstayn, L., Milly, G., Faluvegi, G.,
648   Balkanski, Y., Collins, W. J., Conley, A. J., Dalsoren, S., Easter, R., Ghan, S., Horowitz, L., Liu, X., Myhre, G., Nagashima, T., Naik, V.,
649   Rumbold, S., Skeie, R., Sudo, K., Szopa, S., Takemura, T., Voulgarakis, A., and Yoon, J.-H.: Radiative forcing in the ACCMIP historical
650   and future climate simulations, Atmospheric Chemistry and Physics, https://doi.org/doi:10.5194/acpd-12-21105-2012, 2012.

651 Shine, K., Berntsen, T., Fuglestvedt, J., and Sausen, R.: Scientific issues in the design of metrics for inclusion of oxides of nitrogen in global
652   climate agreements, PNAS, 102, 15 768–15 773, https://doi.org/10.1073/pnas.0506865102, 2005.

653 Stier, P., Feichter, J., Kloster, S., Vignati, E., and Wilson, J.: Emission-induced nonlinearities in the global aerosol system: Results from the
654   ECHAM5-HAM aerosol-climate model, Jornal of Climate, 19, 3845–3862, https://doi.org/10.1175/JCLI3772.1, 2006.

Atmospheric
Chemistry
and Physics
Discussions

Open Access

655 Stier, P., Schutgens, N. A. J., Bellouin, N., Bian, H., Boucher, O., Chin, M., Ghan, S., Huneeus, N., Kinne, S., Lin, G., Ma, X., Myhre, G.,

656   Penner, J. E., Randles, C. A., Samset, B., Schulz, M., Takemura, T., Yu, F., Yu, H., and Zhou, C.: Host model uncertainties in aerosol

657   radiative forcing estimates: results from the AeroCom Prescribed intercomparison study, Atmospheric Chemistry and Physics, 13, 3245–

658   3270, https://doi.org/10.5194/acp-13-3245-2013, 2013.

659 Wilcox, L. J., Highwood, E. J., Booth, B. B. B., and Carslaw, K. S.: Quantifying sources of inter-model diversity in the cloud albedo effect,

660   Geophysical Research Letters, 42, 1568–1575, https://doi.org/10.1002/2015GL063301, 2015.

Atmospheric
Chemistry
and Physics
Discussions

Table 1. Latitudinal bands definition and region definitions.

Name	Latitudes or region definition
SHext	90°S-28°S
Tropics	28°S-28°N
NHml	28°N-60°N
ARCT	60°N-90°N
AR	66°N-90°N
EU	Europe - HTAPv2
NA	North America - HTAPv2
EA	East Asia - HTAPv2
SA	South Asia - HTAPv2

Table 2. Global results from the experiment where SO_2 emissions in different regions are changed. Units are 10^{-2}K/TgSyr^{-1} for temperature and 10^{-2}Wm^{-2}/TgSyr^{-1} for RF and ERF.

Experiment	0xEU SO_2	7xEU SO_2	5xNA SO_2	5xEA SO_2	10xSA SO_2
$\Delta T/\Delta em$	-1.28	-0.56	-0.61	-0.58	-0.58
$RF/\Delta em$	-1.30	-1.04	-1.22	-1.14	-1.68
$ERF/\Delta em$	-2.55	-0.78	-1.29	-1.00	-0.88

Atmospheric
Chemistry
and Physics
Discussions

Open Access

Table 3. Standard deviations for the different normalised basis quantities evaluated in Figure 4b (unitless).

Variable	EM	IRF	ERF	CB
Increased emissions	0.03	0.15	0.19	0.17
All experiments	0.46	0.43	0.19	0.51

Atmospheric
Chemistry
and Physics
Discussions

Table 4. Regional radiative forcing (RF) and effective radiative forcing (ERF) in Wm^{-2} used to derive latitudinal ARTPs in Fig. 10-13.

Experiment	0xEU SO$_2$	7xEU SO$_2$	5xNA SO$_2$	5xEA SO$_2$	10xSA SO$_2$
RF					
SH	0.000	-0.003	-0.003	-0.024	-0.038
TROP	0.037	-0.239	-0.224	-0.388	-0.685
NHml	0.329	-1.423	-1.415	-1.315	-0.729
ARCT	0.171	-0.859	-0.488	-0.413	-0.143
ERF					
SH	0.729	0.608	0.663	0.511	0.628
TROP	0.081	-0.170	-0.415	-0.330	-0.489
NHml	-0.184	-1.774	-1.710	-1.752	-0.904
ARCT	-0.139	-1.046	-0.900	-1.075	-0.149

Atmospheric
Chemistry
and Physics
Discussions
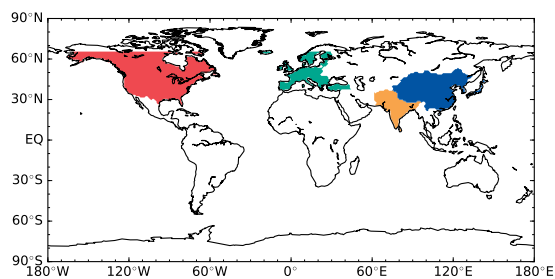
Figure 1. Emission regions according to the HTAP definition. The colours represent: green - Europe (EU), red - North America (NA), blue - East Asia (EA) and yellow - South Asia (SA).

Atmospheric
Chemistry
and Physics
Discussions
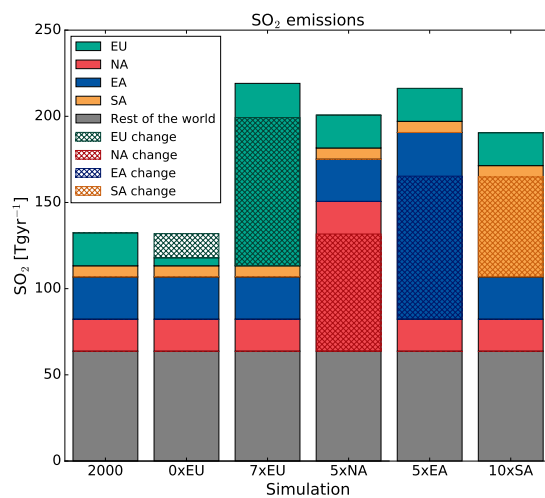
Figure 2. Global annual SO_2 and regional emissions and emission differences in the simulations. Each column shows the total global SO_2 emissions in each simulation and the colour shading indicates the contribution from each region. Hatching indicates the emission change relative to the year 2000 simulation.
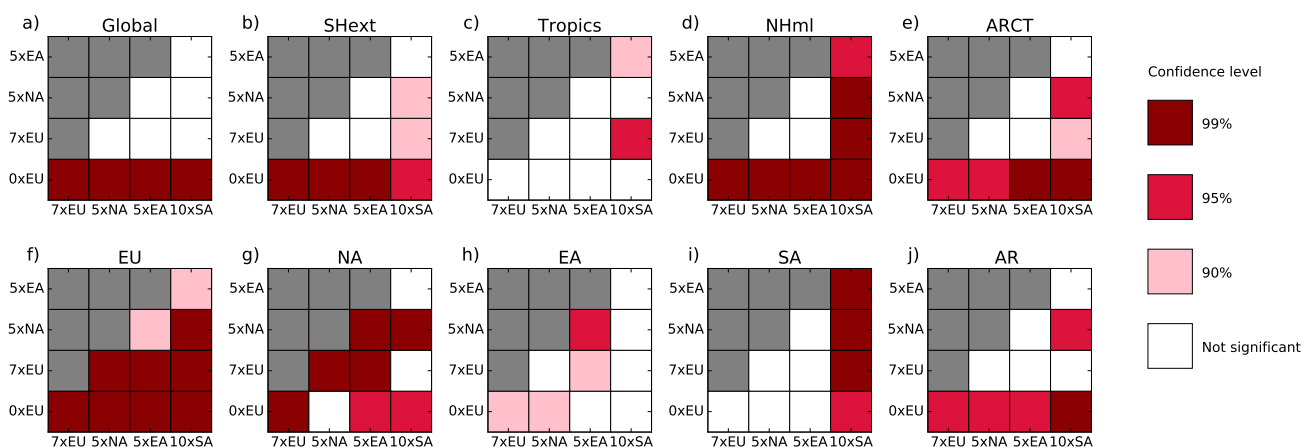
Figure 3. Significance levels for temperature differences between the different experiments, for the temperature response regions a) global mean, b) SHext, c) Tropics, d) NHml, e) ARCT, f) EU, g) NA, h) EA, i) SA and j) AR.
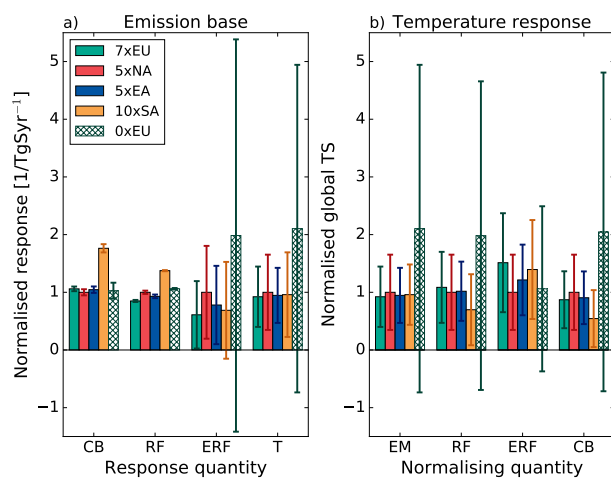
Figure 4. Normalised a) column burden (CB), radiative forcing (RF), effective radiative forcing (ERF) and temperature (T) per unit SO$_2$ emission, and b) normalised temperature response per emissions, RF, ERF and CB in the different experiments. The error indicate show one standard deviation.

Atmospheric
Chemistry
and Physics
Discussions
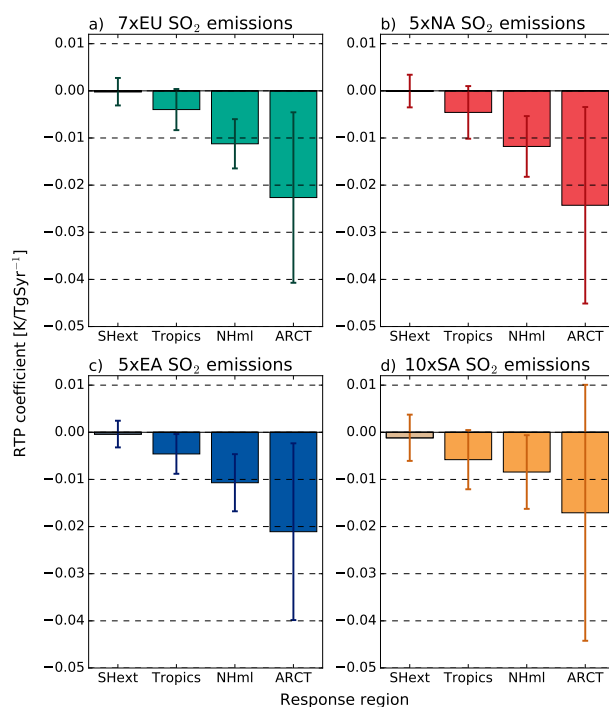
Figure 5. Latitudinal RTP coefficients for SO_2 emission [K/TgSyr^{-1}] for a) EU emissions b) NA emissions c) EA emissions and d) SA emissions. Grey shading indicates that the temperature change is not statistically significant ($p > 0.05$) compared to the control simulation. The error bars indicate one standard deviation.

Atmospheric
Chemistry
and Physics
Discussions
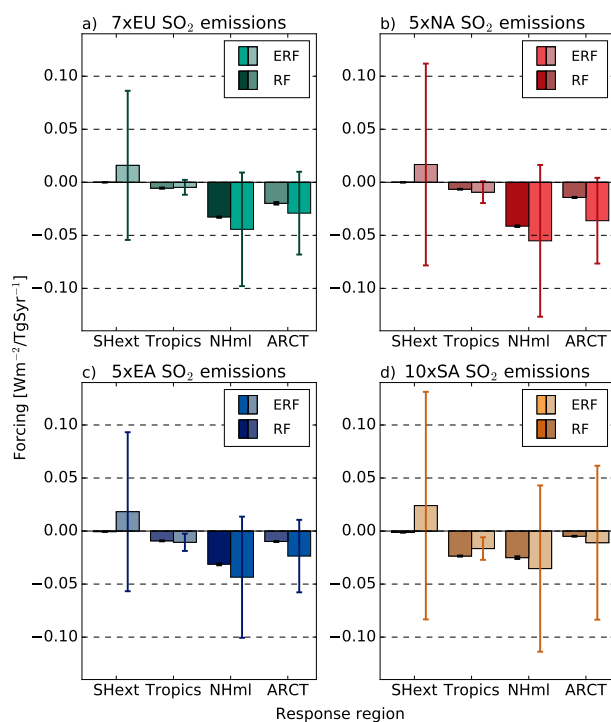
Figure 6. Latitudinal RF and ERF for SO_2 emission [$Wm^{-2}/TgSyr^{-1}$] for a) EU emissions b) NA emissions c) EA emissions and d) SA emissions. In each pair of bars the left bar indicated RF and the right bar indicated ERF. Grey shading indicates that the forcing response is not statistically significant ($p > 0.05$) compared to the control simulation.
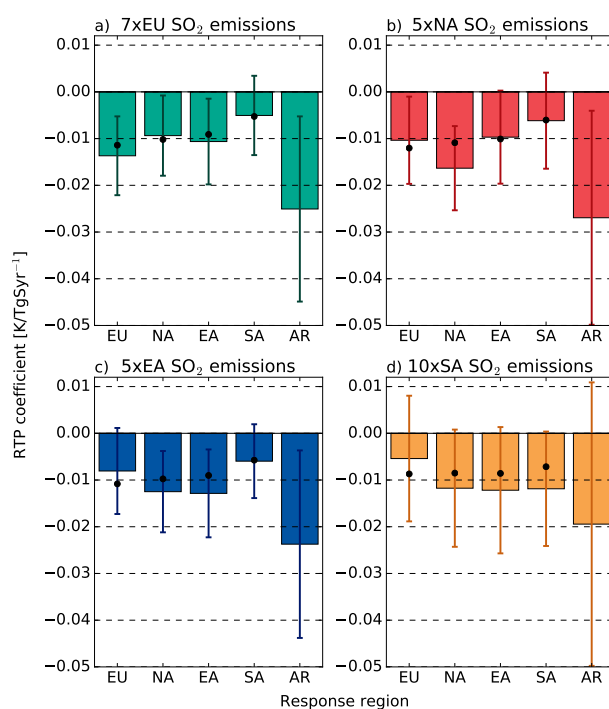
Figure 7. Regional RTP coefficients for SO_2 emission [K/TgSyr^{-1}] for a) EU emissions b) NA emissions c) EA emissions and d) SA emissions. Grey shading indicates that the temperature change is not statistically significant ($p > 0.05$) compared to the control simulation. The error bars indicate one standard deviation. Black dots indicate the zonal mean for the latitudes that cover each region.
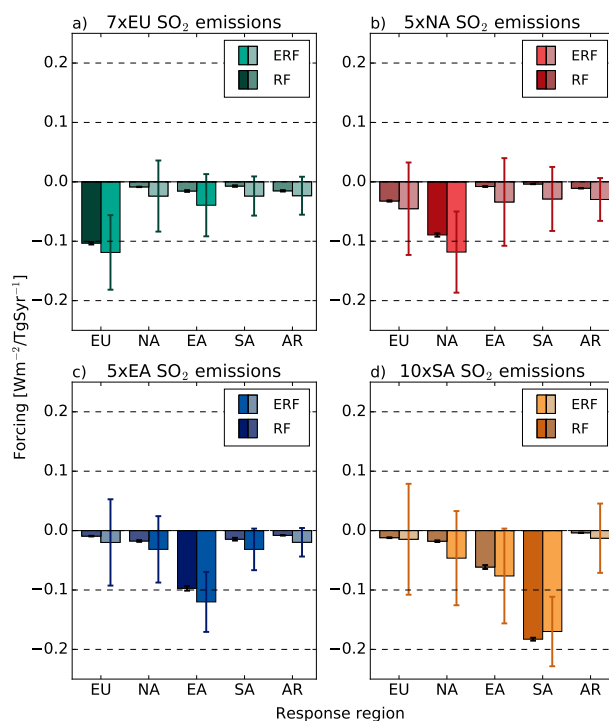
Figure 8. Regional RF and ERF for SO_2 emission [$Wm^{-2}/TgSyr^{-1}$] for a) EU emissions b) NA emissions c) EA emissions and d) SA emissions. In each pair of bars the left bar indicated RF and the right bar indicated ERF. Grey shading indicates that the forcing response is not statistically significant ($p > 0.05$) compared to the control simulation. The black dots indicate the zonal mean of the latitudes covering each response region.
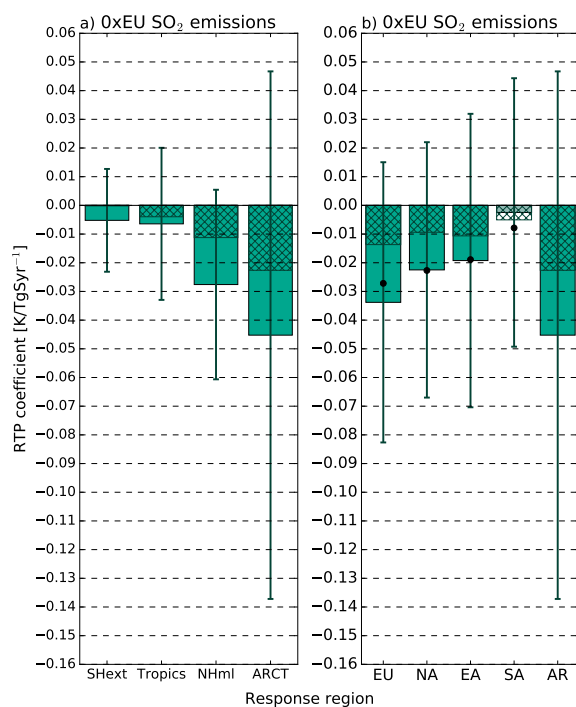
Figure 9. Latitudinal (a) and regional (b) RTP coefficients for 0xEU SO_2 emissions. [K/TgSyr^{-1}]. Grey shading indicates non-statistical differences ($p > 0.05$). The hatching indicated the RTP for 7xEU emissions (cf. Fig. 5 and 7) for easy comparison.

Atmospheric
Chemistry
and Physics
Discussions
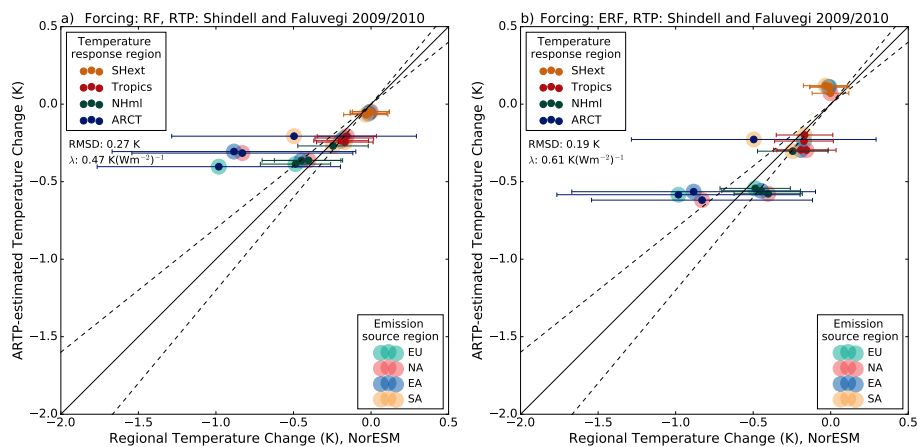
Figure 10. Regional temperature change from the coupled simulations (horizontal axis) compared with the estimated temperature response when using a) RF and b) ERF in combination with the RTP coefficients of Shindell and Faluvegi (2009), Eq. 1 with the climate sensitivity derived from the current experiments (vertical axis). The horizontal bars indicate one standard deviation for the temperature response in the coupled simulations. The dashed lines show ±20% agreement threshold.
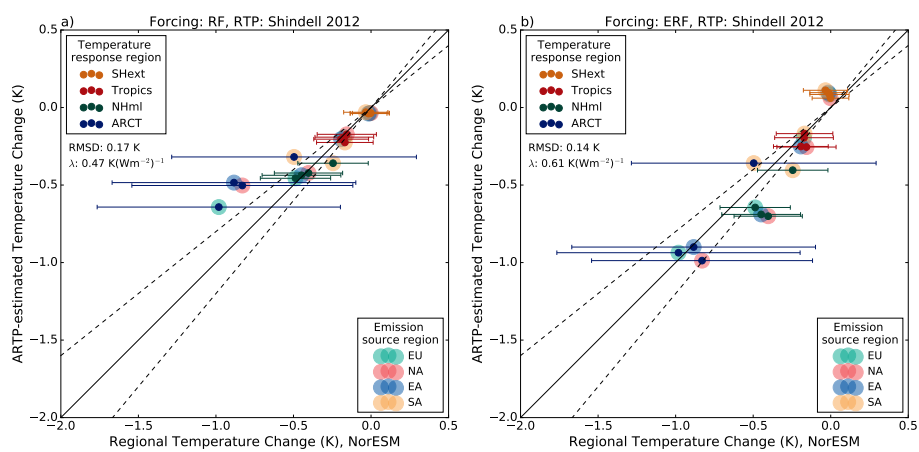
Figure 11. As Fig. 10 but with the RTP coefficients of Shindell (2012), Eq. 2 with the climate sensitivity derived from the current experiments.
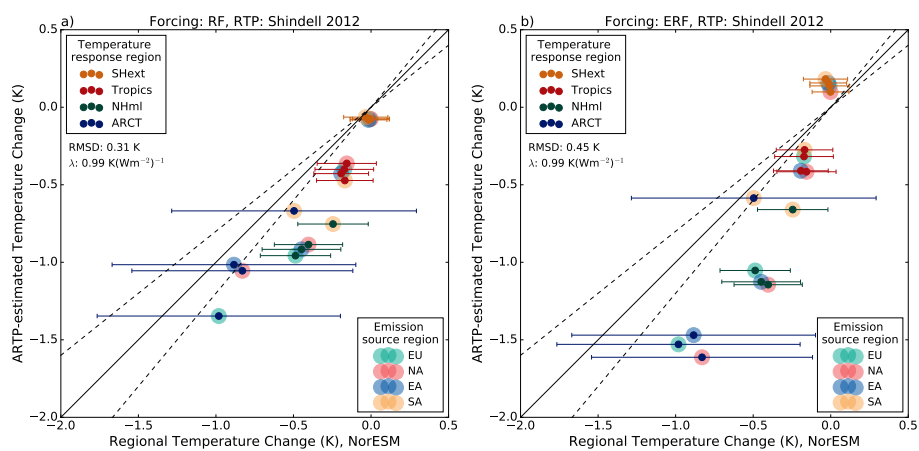
Figure 12. As Fig. 10 but with the RTP coefficients of Shindell (2012), Eq. 2 with the CO_2 sensitivity from Iversen et al. (2013).
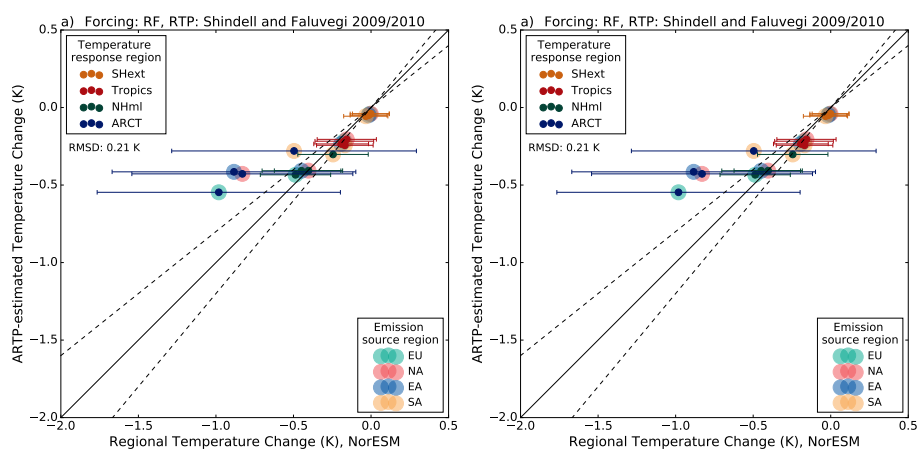
Figure 13. As Fig. 10 but with the RTP coefficients of Shindell and Faluvegi (2009), and with no climate sensitivity applied.